Research Article

Yunfeng Liu*, Lili Chen, Yongfan Tang, Xingde Zhang, and Zhengsong Qiu

Synthesis and characterization of nano-SiO_2@octadecylbisimidazoline quaternary ammonium salt used as acidizing corrosion inhibitor

https://doi.org/10.1515/rams-2022-0006
received September 09, 2021; accepted November 07, 2021

Abstract: Aiming at the current situation that the existing acidizing corrosion inhibitors are difficult to apply in high temperature, high concentration acid, and other complex conditions, this article uses nano-SiO_2 as the core and preferably functional monomers to synthesize nano-SiO_2@octadecylbisimidazoline quaternary ammonium salt (nano-SiO_2@OBQA). Analytical methods such as nuclear magnetic resonance, infrared, and scanning electron microscopy were used for characterization. The corrosion inhibition performance of the N80 steel sheet by nano-SiO_2@OBQA in 20% concentrated hydrochloric acid was studied using the high-temperature corrosion testing machine and adsorption isotherm model combined with quantum chemistry calculations to explore its mechanism of action. The results show that nano-SiO_2@OBQA has good high-temperature resistance. When the temperature is 180°C and the dosage of nano-SiO_2@OBQA is 4%, the corrosion inhibition rate is 61.42 $g \cdot m^{-2} \cdot h^{-1}$. Studies have shown that the adsorption of nano-SiO_2@OBQA on the surface of the N80 steel sheet follows the Langmuir isotherm adsorption model, which is spontaneous chemical adsorption.

Keywords: acidizing corrosion inhibitor, nano-SiO_2, imidazoline, quaternary ammonium salt, isothermal adsorption, quantum chemistry

1 Introduction

With the development of drilling engineering, the number of deep wells and ultra-deep wells has increased, and the bottom hole environment is gradually becoming more complicated, which puts forward higher requirements for the production of stimulation techniques such as acid fracturing [1–5]. In the oilfield development process, the pickling liquid can effectively increase the output of crude oil, but its corrosion of tubing and other equipment also brings additional operating costs [6,7]. At present, adding acidizing corrosion inhibitor is the most commonly used method of anti-corrosion [8–10], but it has been studied more in low-temperature and low-concentration acid solutions, and less research in high-temperature and high-concentration acid solutions [11]. Therefore, acidizing corrosion inhibitors with high-temperature resistance and high concentration acid resistance have become a problem that needs to be solved urgently.

There are three main methods of anti-corrosion. First, the corrosion can be controlled from the source, that is the development of high-corrosion-resistant metals or the addition of corrosion-resistant elements [12,13]. Second, a layer of anti-corrosion paint can be applied to the metal surface to isolate the metal from the corrosive environment [14,15]. In the third aspect, acidizing corrosion inhibitors can be added [16]. This method is the easiest to operate, cheapest, and effective, but it also has problems such as high toxicity and difficult degradation [17,18]. Based on this, the development of low-toxic and easily degradable acidizing corrosion inhibitors is particularly important [19]. Imidazoline acidizing corrosion inhibitors

* **Corresponding author: Yunfeng Liu,** Research Institute of Natural Gas Technology, Southwest Oil and Gas Field Company of PetroChina, Chengdu 610213, China, e-mail: lyf6280168@126.com
Lili Chen: Southwest Oil and Gas Field Company of PetroChina, Chengdu 610213, China
Yongfan Tang, Xingde Zhang: Research Institute of Natural Gas Technology, Southwest Oil and Gas Field Company of PetroChina, Chengdu 610213, China
Zhengsong Qiu: School of Petroleum Engineering, China University of Petroleum (East China), Qingdao 266580, China
ORCID: Yunfeng Liu 0000-0002-6851-8792

are a commonly used type in oilfields. They can form a film structure on the metal surface through chemical adsorption to prevent direct contact between acid and metal. At the same time, imidazoline acidizing corrosion inhibitors have the advantages of low toxicity, high efficiency, and excellent thermal stability [20–22]. Therefore, imidazoline acidizing corrosion inhibitors are widely used in oil and gas field development projects.

The application of nanomaterials has improved efficiency for oil and gas field development projects [23,24], especially the treatment agent with a "core–shell" structure obtained by combining inorganic and organic materials. This can be explained by the nanomaterials providing a rigid skeleton structure for the polymer. On the one hand, it can improve the temperature resistance of the polymer. On the other hand, it can enter the fracturing channel and play the role of supporting the channel. Therefore, the research and development of acidizing corrosion inhibitors with the framework of inorganic nanomaterials have great significance.

2 Materials and methods

2.1 Materials

Azelaic acid (CAS:123-99-9), analytical grade, was purchased from Shanghai Macleans Biochemical Technology Co., Ltd. *N*-(2-Hydroxypropyl)ethylenediamine (CAS:102-60-3), analytical grade, was bought from Jiangsu Aikang Biomedical R&D Co., Ltd. Xylene (CAS:1330-20-7), analytical grade, was from Shanghai Macleans Biochemical Technology Co., Ltd. Acetone, absolute ethanol, and Al_2O_3, analytically pure, were purchased from Shanghai Aladdin Biochemical Technology Co., Ltd. 4-Methoxy-3-methylbenzyl chloride, chemically pure, was purchased from Beijing Hanlongda Technology Development Co., Ltd. 4-Methoxy-3-methyl-1-chloromethane-cyclohexane, industrial grade, was from Weifang Qianjin Fine Chemical Co., Ltd.

2.2 Synthesis of nano-SiO_2@octadecylbisimidazoline quaternary ammonium salt

2.2.1 Surface coating of nano-SiO_2 microspheres

Disperse 0.05 mol nano-SiO_2 microspheres in 200 mL of deionized water solution, slowly add 0.2 mol azelaic acid dropwise, stir at 300 rpm at 20°C for 3 h, filter and freeze-dry to obtain nano-SiO_2 microspheres coated with azelaic acid.

2.2.2 Synthesis of nano-SiO_2@bisimidazoline intermediate

Put the product obtained in step (1) into a 500 mL three-necked flask equipped with an electric stirrer, a water separator, and a spherical condenser and then slowly add 10 mL of xylene at 5 mL·min^{-1}, and add 0.01 mol of the catalyst Al_2O_3, Stir for 20 min, then slowly add 0.5 mol of *N*-(2-hydroxypropyl)ethylenediamine into the system with a constant pressure drop funnel, and reflux at 170°C for 6 h, then react at 190°C for 10 h. Use a rotary evaporator to evaporate and remove toluene at 150°C to obtain a bisimidazoline quaternary ammonium salt intermediate (Figure 1).

2.2.3 Quaternization reaction

Disperse 0.2 mol of bisimidazoline quaternary ammonium salt intermediate in 250 mL of absolute ethanol to fully dissolve it, and add 0.5 mol of 4-methoxy-3-methylbenzyl chloride at 40–50°C for quaternization. After reacting for 2–4 h, the absolute ethanol is distilled out under reduced pressure, and then recrystallized three times with a mixed solution of ethanol and acetone in an ice-water bath, and dried in a vacuum drying oven to obtain the final product nano-SiO_2@octadecylbisimidazoline quaternary ammonium salt (SiO_2@OBQA) (Figure 2).

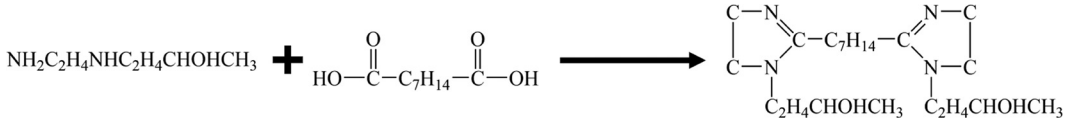

Figure 1: Synthesis of nano-SiO_2@bisimidazoline intermediate.

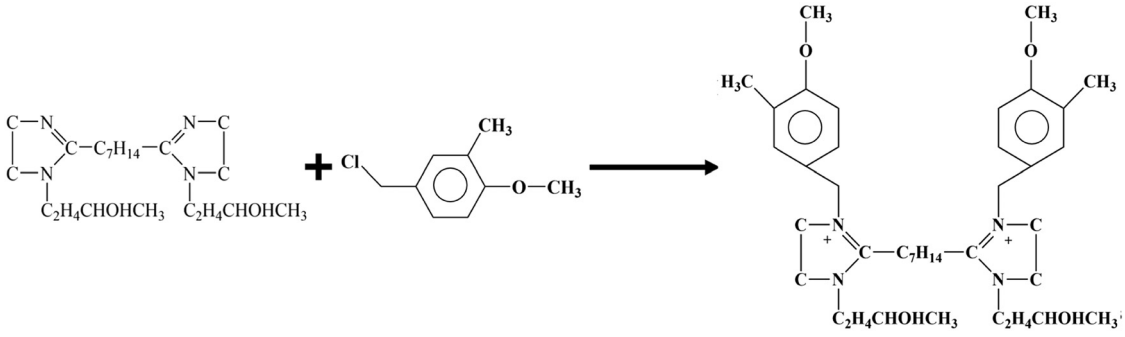

Figure 2: Quaternization reaction.

2.3 Characterization of physical and chemical properties

The nano-SiO_2@OBQA was analyzed by infrared spectroscopy (resolution 4 cm^{-1}, wavenumber range 4,000–400 cm^{-1}, and scanning number 32) using American Thermo Fisher Nicolet IS5 FT-IR spectrometer. ^{1}H-NMR analysis was performed on nano-SiO_2@OBQA with a German Bruker AVANCE III 500 MHz nuclear magnetic resonance spectrometer (resolution ≤ 0.2 Hz, sensitivity 390:1 [5 mm 0.1% EB]). The thermal stability of nano-SiO_2@OBQA was evaluated using the TG/DTA7300 thermogravimetric dual analyzer of Japan HITACHI company (the test temperature range is 20–600°C, the heating rate is 10°C·min^{-1}, and the test gas atmosphere is N_2). The microstructure of nano-SiO_2@OBQA was characterized by the S-4800 SEM analyzer of Hitachi.

2.4 Evaluation of corrosion inhibition performance

Taking the N80 steel sheet as the corrosion test piece, the influence of temperature and nano-SiO_2@OBQA concentration on corrosion inhibition performance was explored. The experiment uses two sets of parallel experiments to eliminate accidental errors and calculates the corrosion inhibition rate according to formula (1).

$$\eta = \frac{v_0 - v}{v_0} \times 100\%, \quad (1)$$

where η – corrosion inhibition rate, %. v – corrosion rate of steel sheet after adding acidizing corrosion inhibitor, g·m^{-2}·h^{-1}, v_0 – corrosion rate of steel sheet in acid, g·m^{-2}·h^{-1}.

2.5 Quantum chemistry research

Using the Chem3D Ultra program and the Huckel molecular orbital theory, the molecular structure optimization and quantum chemical calculations of the nano-SiO_2@OBQA molecule are carried out.

3 Results and discussion

3.1 Molecular structure characterization

3.1.1 FT-IR analysis

It can be seen from Figure 3 that 3401.13 cm^{-1} is the stretching vibration peak of –OH, 2924.04 and 2853.65 cm^{-1} are the

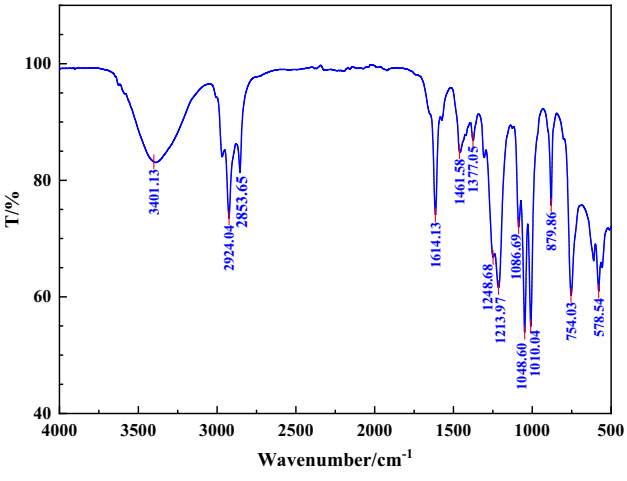

Figure 3: FT-IR analysis of emulsifier nano-SiO_2@OBQA.

stretching vibration peaks of $-CH_3$ and $-CH_2$, respectively, and 1614.13 cm^{-1} is the stretching vibration of C=N. Peaks 1,461 and 1374.62 cm^{-1} are the stretching vibration peaks of C–H, 1213.00 and 1086 cm^{-1} are the stretching vibration peaks of C–N, 1010.04 cm^{-1} is the stretching vibration peak of C–O, 879.86 and 754.03 cm^{-1} are the characteristic peaks of the mono-substituted benzene ring. Therefore, it can be explained that nano-SiO_2@OBQA was successfully synthesized.

3.1.2 ^{1}H-NMR analysis

It can be seen from Figure 4 that nano-SiO_2@OBQA mainly has nine kinds of absorption peaks, including nine kinds of hydrogen atoms. 0–2 ppm is alkane structure, 2–4 ppm is CH–NH_2, hydroxyl structure, and 7.28 ppm is benzene ring structure. Among them, the absorption peak area with a chemical shift of 1.24 ppm is larger, indicating that the carbon chain in the alkane structure is longer, which can improve the temperature resistance of the imidazoline quaternary ammonium salt to a certain extent. The chemical shift of 2–4 ppm shows that an imidazoline ring is formed. At the same time, the addition ratio of azelaic acid and *N*-(2-hydroxypropyl)-ethylenediamine is 2:5, ensuring that azelaic acid can be combined with *N*-(2-hydroxypropyl)-ethylenediamine fully reacted to form a bisimidazole ring, which also shows that the imidazoline quaternary ammonium salt was successfully synthesized. The absorption peak with a chemical shift of 7.28 ppm indicates the presence of a benzene ring in the structure, which further improves the temperature resistance of the bisimidazoline quaternary ammonium salt.

3.1.3 Thermogravimetric analysis (TGA)

It can be seen from Figure 5 that the first mass loss of about 20% occurs in the range of room temperature to 100°C, which is mainly caused by the gradual evaporation of adsorbed water and bound water in the sample. At this time, the large mass loss rate is mainly due to the bisimidazoline intermediate produced by the reaction of azelaic acid and *N*-(2-hydroxypropyl)-ethylenediamine with benzyl chloride. Among them, the molar ratio of azelaic acid to *N*-(2-hydroxypropyl)-ethylenediamine is 2:5, and excess *N*-(2-hydroxypropyl)-ethylenediamine can ensure that two steps of dehydration will occur before the final formation of bisimidazoline. When the temperature is 100–300°C, the methoxy group and the methyl group on the molecular branch of the emulsifier will be broken, and the second mass loss rate is about 8.0%. When the temperature is 300–500°C, the mass loss rate is about 50%. The mass loss is mainly caused by the rupture of the imidazoline ring and main chain in the molecular structure of the emulsifier. The maximum mass loss occurs at 330°C. The results show that the bisimidazoline quaternary ammonium salt emulsifier nano-SiO_2@OBQA has better thermal stability.

3.1.4 Microstructure characterization

The result is shown in Figure 6. The particle size of nano-SiO_2@OBQA is 2–5 μm, the particle size distribution is uniform, the sphericity is excellent, and there is adhesion between a small number of particles as shown in Figure 6(b). This may be due to the synthesis process of bisimidazoline,

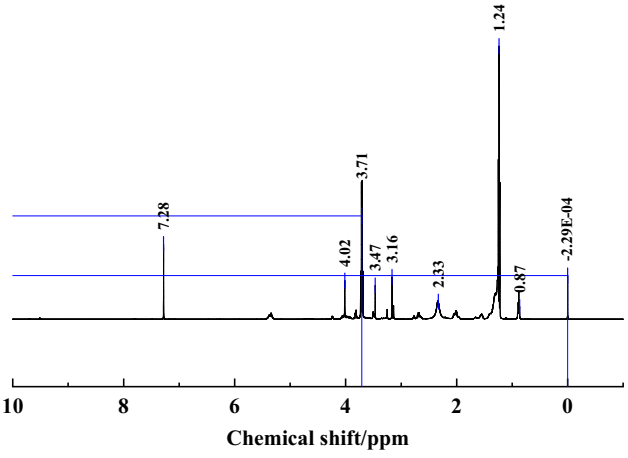

Figure 4: ^{1}H-NMR analysis of emulsifier nano-SiO_2@OBQA.

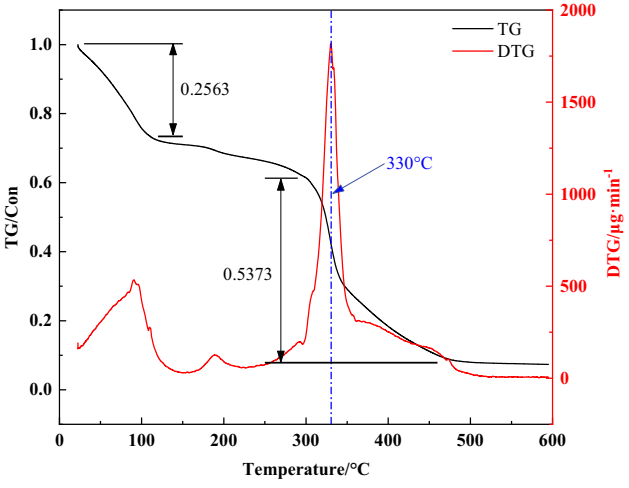

Figure 5: TG and DTG analysis of nano-SiO_2@OBQA.

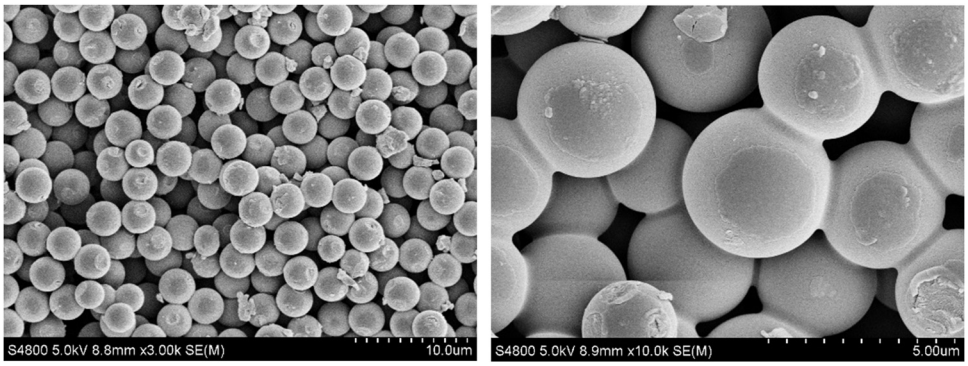

Figure 6: The scanning electron microscopy image of nano-SiO_2@OBQA (left: 3,000×; right: 10,000×).

the SiO_2 microspheres adhere to each other by adsorption. This can indicate that the octadecylbisimidazoline quaternary ammonium salt successfully coated SiO_2.

3.2 Quantum chemistry research

Chooto believes that during the reaction of molecules, molecular orbitals interact, and frontal orbitals have priority [25]. For acidizing corrosion inhibitors, it is generally believed that quantization parameters such as the highest occupied orbital energy E_{HOMO} and the lowest occupied orbital energy E_{LUMO} can characterize the interaction between acidizing corrosion inhibitor molecules and metal atoms. Among them, the HOMO orbital represents the ability to provide monads, the LUMO orbital represents the ability to accept electrons, and the difference between the energy of the HOMO orbital and the LUMO orbital is the energy gap, which is used to characterize the difficulty of chemical reactions [26].

Huckel analysis orbital theory is used to optimize the molecular structure and quantum chemical calculations of nano-SiO_2@OBQA. As shown in Figure 7, the imidazoline and the vicinity of the benzene ring on the right side of the acidizing corrosion inhibitor have a higher ability to donate electrons, and the vicinity of the benzene ring on the left side has a higher ability to accept electrons, indicating that the acidizing corrosion inhibitor has the ability to acquire and lose electrons, and form chemical adsorption with atoms on the metal surface, reducing the corrosion of the metal by the acid solution. At the same time, the energy range (ΔE) is 1.087 eV, indicating that the reaction is easier. As shown in Table 1, the value of ($E_{LUMO,SiO_2@OBQA} - E_{HOMO,Fe}$) is greater than the value of ($E_{LUMO,Fe} - E_{HOMO,SiO_2@OBQA}$), and the difference is greater than 3 eV, indicating that the tendency of the acidizing

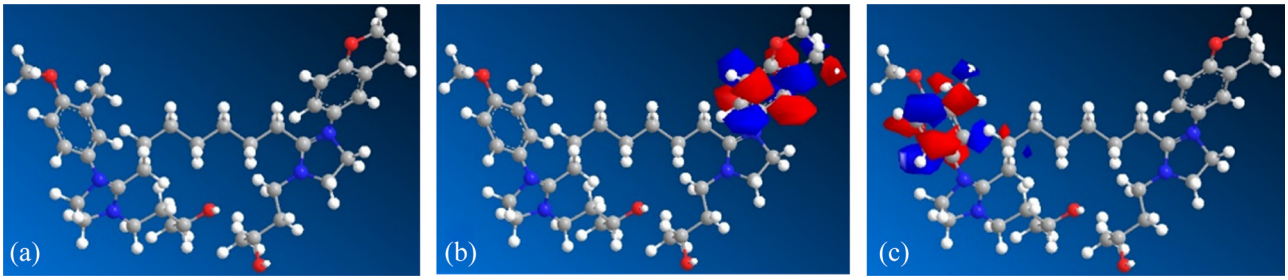

Figure 7: Optimized structure (a), HOMO (b), and LUMO (c) distributions of nano-SiO_2@OBQA.

Table 1: Frontier orbital energies of nano-SiO_2@OBQA

Molecular	E_{HOMO} (eV)	E_{LUMO} (eV)	$E_{LUMO,SiO_2@OBQA} - E_{HOMO,Fe}$ (eV)	$E_{LUMO,Fe} - E_{HOMO,SiO_2@OBQA}$ (eV)	ΔE (eV)
SiO_2@OBQA	−0.631	0.456	8.266	0.381	1.087
Fe	−7.81	−0.25	—	—	—

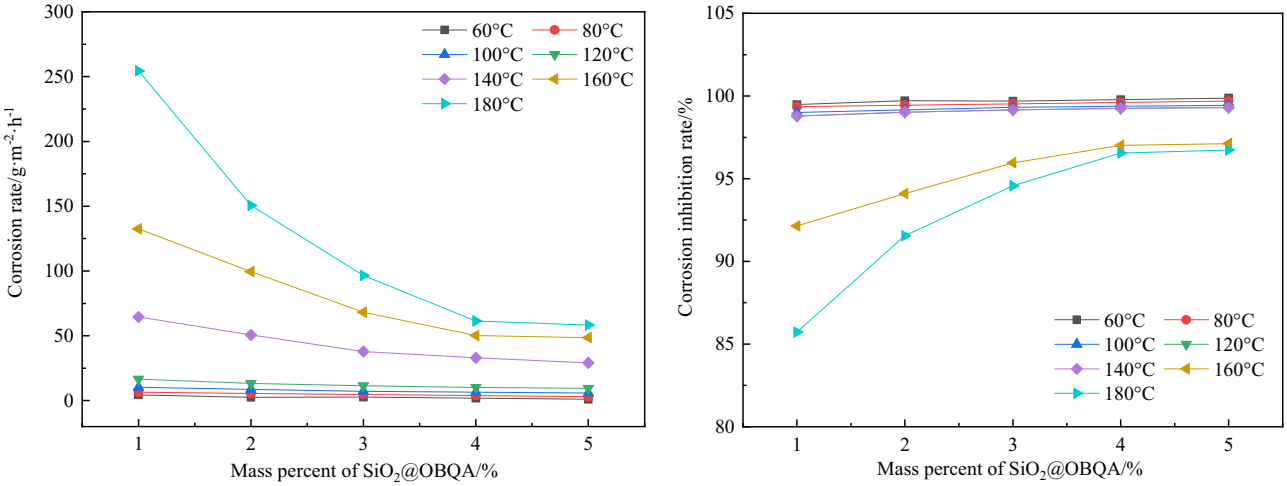

Figure 8: The influence of nano-SiO_2@OBQA concentration on corrosion inhibition performance at different temperatures.

corrosion inhibitor nano-SiO_2@OBQA molecule accepting electrons to interact with Fe is smaller than the tendency to donate electrons to interact with Fe [27].

3.3 Evaluation of corrosion inhibition performance

Different mass fractions of nano-SiO_2@OBQA were added to 400 mL 20% hydrochloric acid solution. The corrosion of the N80 steel sheet was tested at different temperatures within 4 h, and its adsorption performance was characterized.

The corrosion rate and corrosion inhibition rate are shown in Figure 8. When the temperature is constant, the corrosion rate decreases as the concentration of nano-SiO_2@OBQA increases. This is because nano-SiO_2@OBQA can adhere to the surface of the N80 steel sheet to form a protective layer to inhibit acid corrosion. As the concentration of nano-SiO_2@OBQA increases, the area attached to the N80 steel sheet also increases. When the concentration is constant, the surface coverage reaches the maximum. With the increase of the amount of the inhibitor, the corrosion rate first drops sharply and then tends to be stable. When the concentration of nano-SiO_2@OBQA is constant, the corrosion rate increases as the temperature increases. This is caused by the thermal movement of molecules. Chooto and Manaboot believes that the increase in temperature helps to increase the absorption rate of inhibitor molecules [25], but the molecular movement of the acid will also increase with the increase in temperature. At the same time, Schmid found that metal surfaces included in organic molecules also undergo corrosion reactions, but the reaction rate is lower than that of bare metal surfaces [28]. Therefore, this can also explain the abovementioned experimental phenomenon.

3.4 Adsorption isotherm model

The isothermal adsorption model of nano-SiO_2@OBQA was constructed, and the Gibbs free energy ΔG°_{ads} was calculated by the formula to characterize the spontaneity of the adsorption process and the stability of the adsorption layer on the steel surface. It can be seen from Figure 9 and Table 2 that the size of R^2 is close to 1, indicating that

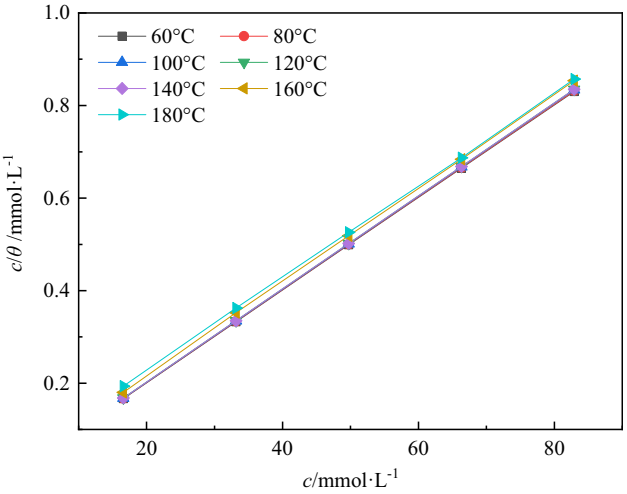

Figure 9: Curves fitting of the corrosion data for steel at different temperatures.

Table 2: The isotherm fitting parameters

T (K)	Intercept (mmol·L^{-1})	K_{ads} (L·mmol^{-1})	ΔG°_{ads} (kJ·mol^{-1})	R^2
333.15	0.0009	1111.1111	−30.21	1
353.15	0.001	1,000	−31.71	1
373.15	0.0011	909.0909	−33.22	1
393.15	0.0013	769.2308	−34.45	1
413.15	0.0013	769.2308	−36.20	1
433.15	0.014	71.4286	−29.41	0.99
453.15	0.0295	33.8983	−27.97	0.99

the curve fits well and follows the Langmuir isotherm adsorption model. The Gibbs free energy is negative, indicating that the adsorption process between the organic molecules and the steel sheet is spontaneous and stable. Generally, when the value of ΔG°_{ads} is about −20 kJ·mol^{-1}, the steel sheet and the organic molecules interact through electrostatic at this time. When the value of ΔG°_{ads} is around −40 kJ·mol^{-1}, the steel sheet and organic molecules are adsorbed by chemical interaction [29–32]. According to the table, the range of ΔG°_{ads} of nano-SiO_2@OBQA is between −28 and −37 kJ·mol^{-1}, indicating that the two are mainly through chemical adsorption. As the temperature increases, the Gibbs free energy first decreases and then increases, indicating that the adsorption capacity first increases and then decreases. This can also explain the rapid increase in the corrosion rate when the temperature is greater than 120°C. Combined with the results of quantum chemistry, it can be considered that the mechanism of action of nano-SiO_2@OBQA can be deduced. The π electrons of the benzene ring, the unbound electron pairs of oxygen in the methoxy group, the C═N double bond on the bisimidazoline ring, and the N atom with a lone pair of electrons can all provide electrons and then covalently with the metal surface.

3.5 Mechanism discussion

According to the microscopic characterization and performance evaluation, the molecular mechanism of nano-SiO_2@OBQA mainly includes two aspects: adsorption mechanism and temperature resistance mechanism as shown in Figure 10. Generally, the temperature resistance of the polymer can be improved by increasing the rigidity of the main chain and the side chain. The nano-SiO_2@OBQA molecule synthesized has good thermal stability because of the long carbon chain and the benzene ring structure. Meanwhile, the introduction of inorganic nanomaterials will also improve the temperature resistance of molecules to a certain extent [33,34]. Thereby, corrosion inhibition needs to be closely adsorbed with the metal

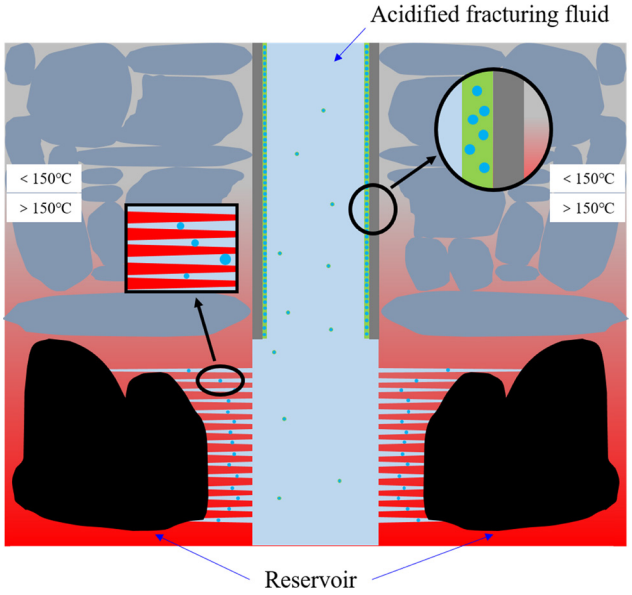

Figure 10: The mechanism of nano-SiO_2@OBQA (the color of the formation changes from gray to red, indicating that the temperature of the formation increases with the increase in depth).

under different well conditions, generally divided into physical adsorption and chemical adsorption. On the one hand, the nano-SiO_2@OBQA molecule contains a longer alkyl hydrophobic chain, which greatly enhances the hydrophobicity of the nano-SiO_2@OBQA molecule and improves the density of the molecular film of the acidizing corrosion inhibitor on the metal surface. On the other hand, the π electron of the benzene ring, the unbound electron of the oxygen in the methoxy group, the C═N double bond on the bisimidazoline ring, and the N atom with a lone pair of electrons can provide electrons and then occur covalent effect on the metal surface. The combination forms π–d coordination bonds that enhances the activation energy of the metal surface and improves the adsorption capacity of the acidizing corrosion inhibitor molecules on the metal surface, thereby helping to form a dense adsorption film, reducing the direct contact between the corrosive medium and the metal.

In the process of acid fracturing, it is generally necessary to add rigid materials to support the reservoir channels. Nano-SiO_2@OBQA has a rigid core structure and is insoluble in hydrochloric acid. Therefore, it can be used as a proppant to enter the oil reservoir channel, reduce operating costs, and achieve the goal of reducing costs and increasing efficiency.

3.6 Innovation point

At present, there is no report claiming the introduction of inorganic nanomaterials in acidizing corrosion inhibitors.

In this article, the innovative introduction of electrodeless nanomaterials as the "core" structure of acidizing corrosion inhibitors is presented. On the one hand, it can improve the molecular structure strength of the acidizing corrosion inhibitor and improve the thermal stability of the polymer molecules. On the other hand, the acidizing corrosion inhibitor molecules are injected into the formation in acid fracturing operations, so that they can also act as a support channel in the target formation, thereby improving the operating efficiency of acid fracturing.

4 Conclusion

The nano-SiO_2@OBQA can effectively inhibit the corrosion of steel sheets in 20% HCl. At 180°C, when the addition of nano-SiO_2@OBQA is 4%, the corrosion rate is 61.42 $g \cdot m^{-2} \cdot h^{-1}$, and the corrosion inhibition rate reaches more than 95%. The nano-SiO_2@OBQA has excellent corrosion inhibition performance. Studies have shown that the adsorption of nano-SiO_2@OBQA salt on the surface of the N80 steel sheet follows the Langmuir isotherm adsorption model, which is a spontaneous chemical adsorption. At the same time, nano-SiO_2@OBQA can form stable adsorption with metals.

Acknowledgements: All the techniques who have contributed this research should be also expressed our most sincere thanks.

Funding information: This work was financially supported by the Research Project of Southwest Oil and Gas Field Company of PetroChina named "Popularization and application of 180°C high temperature corrosion inhibitor and acid system" (No. 20210302-29) and "Research on autogenous acid at 180°C and its mechanism" (No. 20210302-07).

Author contributions: All authors have accepted responsibility for the entire content of this manuscript and approved its submission.

Conflict of interest: The authors state no conflict of interest.

References

[1] Son, A. J., T. M. Ballard, and R. E. Loftin. Temperature-stable polymeric fluid-loss reducer tolerant to high electrolyte contamination. *SPE Drilling Engineering*, Vol. 2, No. 03, 1987, pp. 209–217.

[2] Akpan, E. U., G. C. Enyi, G. Nasr, A. A. Yahaya, A. A. Ahmadu, and B. Saidu. Water-based drilling fluids for high-temperature applications and water-sensitive and dispersible shale formations. *Journal of Petroleum Science and Engineering*, Vol. 175, 2019, pp. 1028–1038.

[3] Liu, X., R. Jiang, and W. Huang. Experimental study on optimal injection pressure of heavy oil reservoir developed by supercritical CO_2 flooding. *Fresenius Environmental Bulletin*, Vol. 29, No. 4, 2020, pp. 2555–2561.

[4] Luo, X., W. Han, H. Ren, Q. Zhuang. Research on high performance temporary plugging drilling fluid for reservoir protection and field trial. *Fresenius Environmental Bulletin*, Vol. 28, No. 8, 2019, pp. 6290–6298.

[5] Soltani, A., Head. Reliable level of corrosion inhibitor's residual concentration in wet gas-condensate pipelines. Eurocorr 2020 Virtual Conference, 2020.

[6] Shamlooh, M., S. Abdelrady, M. Buasali, and K Farouque. Well integrity protection using corrosion inhibitor treatment system for sour gas producers in Bahrain field. SPE Middle East Oil and Gas Show and Conference, 2019.

[7] Wylde, J. J., Turnern, and M. Austill. Development, testing and field application of a novel combination foamer-iron sulfide scale inhibitor-corrosion inhibitor in East Texas. SPE International Conference on Oilfield Chemistry, 2017.

[8] Danaee, I. and M. N. Khomami. Effect of ethylenediamine on corrosion of AISI 4130 steel alloy in 30% ethylene glycol solution under static and hydrodynamic condition. *Materialwissenschaft Und Werkstofftechnik*, Vol. 43, No. 11, 2012, pp. 942–949.

[9] Vishwanatham, S. and A. Kumar. Corrosion inhibition of mild steel in binary acid mixture. *Corrosion Reviews*, Vol. 23, No. 2–3, 2005, pp. 181–194.

[10] Ghasemi, O., I. Danaee, G. R. Rashed, M. RashvandAvei, and M. H. Maddahy. Inhibition effect of a synthesized N, N'-bis(2-hydroxybenzaldehyde)-1, 3-propandiimine on corrosion of mild steel in HCl. *Journal of Central South University*, Vol. 20, No. 2, 2013, pp. 301–311.

[11] Bentiss, F., M. Lebrini, H. Vezin, and M. Lagrenée. Experimental and theoretical study of 3-pyridyl-substituted 1,2,4-thiadiazole and 1,3,4-thiadiazole as corrosion inhibitors of mild steel in acidic media. *Materials Chemistry and Physics*, Vol. 87, 2004, pp. 18–23.

[12] Scully, J. R., S. B. Inman, A. Y. Gerard, C. D. Taylor, W. Windl, D. K. Schreiber, et al. Controlling the corrosion resistance of multi-principal element alloys. *Scripta Materialia*, Vol. 188, 2020, pp. 96–101.

[13] Duarte, M. J., J. Klemm, S. O. Klemm, K. J. J. Mayrhofer, M. Stratmann, S. Borodin, et al. Element-resolved corrosion analysis of stainless-type glass-forming steels. *Science*, Vol. 341, No. 6144, 2013 Jul 26, pp. 372–376.

[14] Qian, Y., Y. Li, and S. Jungwirth. The application of anti-corrosion coating for preserving the value of equipment asset in chloride-laden environments: a review. *International Journal of Electrochemical Science*, Vol. 10, 2015, pp. 10756–10780.

[15] Cui, G., Z. Bi, R. Zhang, J. Liu, X. Yu, and Z. Li. A comprehensive review on graphene-based anti-corrosive coatings. *Chemical Engineering Journal*, Vol. 373, 2019, pp. 104–121.

[16] Goyal, A., E. Ganjian, H. S. Pouya, and M. Tyrer. Inhibitor efficiency of migratory corrosion inhibitors to reduce corrosion in

reinforced concrete exposed to high chloride environment. *Construction and Building Materials*, Vol. 303, 2021, id. 124461.
[17] Kobzar, Y. L. and K. Fatyeyeva. Ionic liquids as green and sustainable steel corrosion inhibitors: recent developments. *Chemical Engineering Journal*, Vol. 425, 2021, id. 131480.
[18] Baskar, R., H. Lgaz, and R. Salghi. Heterocyclic compounds as corrosion inhibitors for mild steel: a review. *Chemical Science & Engineering Research*, Vol. 1, No. 1, 2019, pp. 32–54.
[19] Saraswat, V. Improved corrosion resistant performance of mild steel under acid environment by novel carbon dots as green corrosion inhibitor. *Colloids and Surfaces A: Physicochemical and Engineering Aspects*, Vol. 627, No. 7, 2021, id. 127172.
[20] Shamsa, A., E. Barmatov, and T. L. Hughes. Hydrolysis of imidazoline based corrosion inhibitor and effects on inhibition performance of X65 steel in CO_2 saturated brine. *Journal of Petroleum Science and Engineering*, Vol. 208(B), 2022, id. 109235.
[21] Shamsa, A., R. Barker, Y. Hua, E. Barmatov, T. L. Hughes, and A. Neville. Performance evaluation of an imidazoline corrosion inhibitor in a CO_2-saturated environment with emphasis on localised corrosion. *Corrosion Science*, Vol. 176, 2020, id. 108916.
[22] Hu, J., Z. H. Zhang, Z. Zhu, J. Chen, X. Hu, and H. Chen. Molecular dynamic simulation and experimental investigation on the synergistic mechanism and synergistic effect of oleic acid imidazoline and l-cysteine corrosion inhibitors. *Corrosion Science*, Vol. 185, 2021, id. 109414.
[23] Jiang, D. S., X. P. Li, K. W. Jiang, B. Chen, and C. Sun. Study on diverting acid conductivity of heterogeneous reservoir in Gaomo area. *Chemical Engineering of Oil & Gas*, Vol. 50, No. 4, 2021, pp. 92–95 + 113.
[24] Xiong, Y., Y. Q. Liu, and Z. H. Mei. Slick water technology of high salinity resistance for shale gas development in Sichuan. *Chemical Engineering of Oil & Gas*, Vol. 48, No. 3, 2019, pp. 62–65 + 71.
[25] Chooto, P. and S. Manaboot. Electrochemical, spectrochemical and quantum chemical studies on dimedone as corrosion inhibitor for copper in acetonitrile. *Journal of Scientific Research & reports*, Vol. 15, No. 2, 2017, pp. 1–13.
[26] Mutombo, P. and N. Hackerman. The effect of some organo-phosphorous compounds on the corrosion behaviour of iron in 6 M HCl. *Anti-corrosion Methods and Materials*, Vol. 45, No. 6, 1998, pp. 413–418.
[27] Song-Qing, H., H. Jian-Chun, F. Cheng-Cheng, M. Si-Qi, Z. Jun, and G. Wen-Yue. Corrosion inhibition of Q235 steel by a novel imidazoline compound under H_2S and CO_2 coexistence. *Acta Physico-chemica Sinica*, Vol. 26, No. 8, 2010, pp. 2163–2170.
[28] Zhong, H. Y., X. Z. Kong, S. Chen, B. Grady, and Z. S. Qiu. Preparation, characterization and filtration control properties of crosslinked starch nanospheres in water-based drilling fluids. *Journal of Molecular Liquids*, Vol. 325, 2021, id. 115221.
[29] Cui, G. D., L. Zhu, Q. Zhou, S. R. Ren, and J. Y. Wang. Geochemical reactions and their effect on CO_2 storage efficiency during the whole process of CO_2 EOR and subsequent storage. *International Journal of Greenhouse Gas Control*, Vol. 108, 2021, id. 103335.
[30] Schmid, G. M. and H. J. Huang. Spectro-electrochemical studies of the inhibition effect of 4, 7-diphenyl-1, 10-phenanthroline on the corrosion of 304 stainless steel. *Corrosion Science*, Vol. 20, No. 8–9, 1980, pp. 1041–1057.
[31] Annand, R. R. Theory of organic corrosion inhibitors adsorption and linear free energy relationships. *Journal of the Electrochemical Society*, Vol. 113, No. 6, 1966, id. 633.
[32] Nakonieczny, D. S., M. Antonowicz, and Z. Paszenda. Surface modification methods of ceramic filler in ceramic-carbon fibre composites for bioengineering applications – a systematic review. *Reviews on Advanced Materials Science*, Vol. 59, No. 1, 2020, pp. 586–605.
[33] Khamis, E., F. Bellucci, R. M. Latanision, and E. S. H. El-Ashry. Acid corrosion inhibition of nickel by 2-(triphenosphoranylidene) succinic anhydride. *Corrosion*, Vol. 47, No. 9, 1991, pp. 677–686.
[34] Bentiss, F., M. Traisnel, N. Chaibi, B. Mernari, H. Vezin, and M. Lagrenée. 2,5-Bis(*n*-methoxyphenyl)-1,3,4-oxadiazoles used as corrosion inhibitors in acidic media: correlation between inhibition efficiency and chemical structure. *Corrosion Science*, Vol. 44, No. 10, 2002, pp. 2271–2289.